Motion of localized disturbances in scalar harmonic lattices

Julia A. Baimova [1] Nikolay M. Bessonov [2] and Anton M. Krivtsov [2,3,*]

[1]*Institute for Metals Superplasticity Problems, Russian Academy of Sciences, Ufa 450001, Russia*
[2]*Institute for Problems in Mechanical Engineering, Russian Academy of Sciences, St. Petersburg 199178, Russia*
[3]*Higher School of Theoretical Mechanics, Peter the Great St. Petersburg Polytechnic University, St. Petersburg 195251, Russia*

We present analytical and numerical investigations of energy propagation in systems of massive particles that interact via harmonic (linear) forces. The particle motion is described by a scalar displacement, and the particles are arranged in a simple crystal lattice. For the systems under consideration we prove the conservation of the total energy flux analytically. Then, using a sample case of a square lattice, we confirm the analytical results numerically. We create disturbances of a special kind which can move with a predefined velocity with a minor change in their shape. We show that a clot of energy, associated with each disturbance, moves similarly to a free body of matter in classical mechanics. We also numerically study a simultaneous propagation of a number of energy clots as an analogy to the motion of point masses in the conventional mechanics of particles. The obtained results demonstrate that an energy flow in lattices can be described in terms of numerous separated energy bodies, making a step towards a linkage between lattice dynamics and the kinetic theory of heat transfer in solids.

I. INTRODUCTION

Energy transfer processes with various natures have been studied widely because of their fundamental and practical implications [1–7]. To date, a number of such processes have been considered in detail, such as the energy transfer between molecules and ions in solids [8], thermal dynamics of nanostructures [9,10], thermal energy transfer [11–15], energy processes in structures subjected to extreme loads [1,2,16], and electromagnetic radiant energy transfer [17]. The theories of mechanical-to-vibrational energy transfer showed that external mechanical impact can be transformed into lattice vibrations, which might further cause damage to the crystal [1–3,18]. A review of the current progress in the field of nonlinear targeted energy transfer is presented in [19]. Wave energy transfer plays an important role in electromagnetic, acoustic, seismic processes [20–27]. The energy transfer in lattices helps to model various physical, mechanical, and biological processes, even in such complex systems as flexible polymers and DNA [28].

Understanding heat transfer processes is of high practical importance, for instance, efficient removal of heat from a reactor core or other high-energy thermal devices [29–31]. Theoretical [32–41] and experimental [42–47] studies showed that at micro- and nanolevels, nondiffusive ballistic and anomalous heat energy transfer is common, especially for low dimensions. This behavior is due to the fact that one of the leading mechanisms of heat transfer in solids is connected to elastic waves, facing fewer obstacles at low scales. Therefore, heat transfer processes in crystalline solids can be effectively described on the basis of kinetic models, in which energy is transferred by phonons, quasiparticles that mimic the properties of material particles [7,11,48–52]. The similarity between mass and energy transfers is well-known, for example, for diffusive processes [53]. However, an analogy between energy transfer and mass transfer for wave processes is still less understood. There are also important results in this area, such as soliton-like solutions for anharmonic systems, that demonstrate explicitly the wave-particle duality [54–56].

Previously, the lattice dynamics approach was successfully used by our group to describe heat transfer in solids, especially on micro- and nanoscales, when the ballistic heat propagation took place [13,14,57–67]. However, kinetic equations, based on the quasiparticle approach, are much simpler than the equations for lattice dynamics and make it possible to obtain visual, easily interpretable solutions [7,11,48,49], allowing us to calculate explicitly such important quantities like kinetic temperature and heat flux [7]. Unfortunately, the transition from dynamics to kinetics is quite complicated and still is not fully understood, especially when considering classical rather than quantum models of solids.

The approach of energy dynamics for describing wave energy transfer in terms of mass transfer is presented in [68] for a one-dimensional system of interacting particles. This approach can be used for various physical phenomena at different scale levels. In the present work, we consider harmonic scalar crystal lattices and analyze the energy transfer by analogy with mass transfer in conventional mechanics. Then, using a sample model of a square lattice, we obtain more detailed formulations and perform computer simulations to confirm the analytical statements.

The general outline of this paper is as follows. An introduction and a brief literature review were given in the present

*Corresponding author: akrivtsov@bk.ru

section. In Sec. II, we introduce the basic quantities and perform an analytical analysis of energy transfer in harmonic scalar lattices. In Sec. III, we apply the results obtained in Sec. II to the case of a square lattice and perform computer simulations. In Sec. IV, we summarize the obtained results. Complex mathematical derivations and formulations are left to Appendixes.

II. SCALAR LATTICES

A. Equation of motion

We consider a set of equal particles, each having mass m. In the reference configuration, the particles are located at the nodes of an ideal crystal lattice. We restrict our consideration to simple infinite lattices—lattices that are shift invariant with respect to a vector connecting any two nodes. These lattices are also inversion invariant: They are centrosymmetric with respect to any node. Vectors connecting a node with neighboring nodes are denoted by $\mathbf{a}_\alpha$, where integer α is a neighbor index. To follow the central symmetry we presume that $\mathbf{a}_{-\alpha} = -\mathbf{a}_\alpha$. All the geometrical information about the particular type of lattice is stored in the set of α numbers and $\mathbf{a}_\alpha$ vectors. The lattice under consideration coincides with its Bravais lattices, and a primitive cell of the lattice contains a single node. This differs from the case of a complex lattice [59], which can be considered a combination of several Bravais lattices, in which a primitive cell contains several nodes; such systems are beyond the scope of the current paper.

The actual state of a particle is determined by a scalar variable $u = u(\mathbf{r})$, where $\mathbf{r}$ is a node position vector. For brevity we call u a displacement, keeping in mind that it is a generalized displacement that can be the displacement, the angle, or some other kinematic variable. Since u is a scalar, the lattice is referred to as a scalar one. The lattice is defined in space of dimension d. The most common case for scalar lattices is $d = 2$; in particular, a two-dimensional (2D) square lattice will be used in this paper as a sample system for computations. However, all analytical results obtained are also valid for $d = 1$, $d = 3$, and even higher dimensions.

The considered system is harmonic; therefore, the interaction between particles is proportional to generalized deformations, which are differences $u(\mathbf{r} + \mathbf{a}_\alpha) - u(\mathbf{r})$. Then the equation of motion takes the form

$$m \frac{d^2 u}{dt^2} = \sum_\alpha C_\alpha [u(\mathbf{r} + \mathbf{a}_\alpha) - u(\mathbf{r})], \quad (1)$$

where t is time, $C_\alpha \equiv C_{-\alpha}$ is an effective stiffness, and the summation is performed over all neighboring particles involved in the interaction.

As an illustrative system, we will consider in this paper an infinite two-dimensional square lattice of identical particles (see Fig. 1). We assume that each particle is connected to its four nearest neighbors by identical elastic massless springs. We study the out-of-plane lattice motions within the framework of the harmonic approximation. In the equilibrium state, the lattice is stretched (the elastic forces are not zero), and the lattice period (the equilibrium distance between the particles) is a. For the square lattice, $\alpha \in \{-2; -1; 1; 2\}$, and the vectors $\mathbf{a}_\alpha$ are $\mathbf{a}_{\pm 1} = \pm a \mathbf{e}_1$ and $\mathbf{a}_{\pm 2} = \pm a \mathbf{e}_2$, where $\mathbf{e}_1$ and $\mathbf{e}_2$ are the
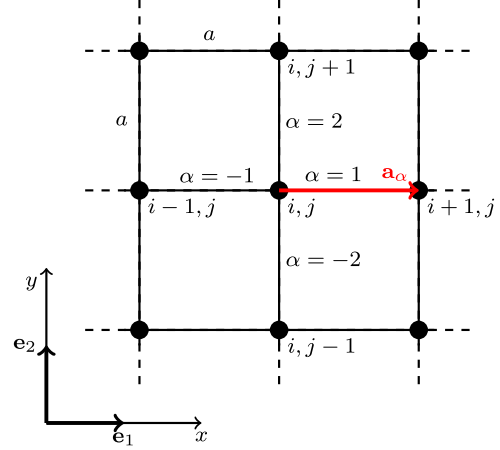

FIG. 1. Sketch of a square lattice with lattice period a and lattice basis vectors $\mathbf{e}_1$ and $\mathbf{e}_2$. The particles are numbered by integer indexes i, j.

unit vectors of the Cartesian basis (see Fig. 1). The position vector $\mathbf{r}$ takes discrete values localized at the lattice nodes. In the case of the square lattice

$$\mathbf{r} \stackrel{\text{def}}{=} a i \mathbf{e}_1 + a j \mathbf{e}_2, \quad i, j \in \mathbb{Z}, \quad (2)$$

where $\mathbb{Z}$ is a set of all integers. With the representation of $\mathbf{r}$ from Eq. (2), the displacement can be written as $u(\mathbf{r}) = u_{i,j}$, which results in the following scalar form of (1) (valid for only the square lattice):

$$\frac{d^2 u_{i,j}}{dt^2} = \frac{C}{m}(u_{i+1,j} + u_{i,j+1} + u_{i-1,j} + u_{i,j-1} - 4u_{i,j}), \quad (3)$$

where C is an effective stiffness, equal to the ratio of the stretching force to the lattice period.

B. Energy and flux

We consider a disturbance of the lattice, which is a deviation of the coordinates and velocities from their equilibrium values. The total energy of the disturbance is

$$E \stackrel{\text{def}}{=} \sum_{\mathbf{r}} \epsilon(\mathbf{r}), \quad (4)$$

where $\epsilon(\mathbf{r})$ is the local energy,

$$\epsilon(\mathbf{r}) \stackrel{\text{def}}{=} \frac{m}{2} v^2(\mathbf{r}) + \frac{1}{4} \sum_\alpha C_\alpha [u(\mathbf{r} + \mathbf{a}_\alpha) - u(\mathbf{r})]^2, \quad (5)$$

and $v \stackrel{\text{def}}{=} \dot{u}$ is the velocity of the particle. The local energy is a sum of the kinetic and potential components, which are proportional to mass m and stiffness C, respectively. The summation in Eq. (4) is done over all the particles in the system; in Eq. (5) it is over all neighbors of the selected particle. As the system is conservative, the total energy of the system is constant: $E = \text{const}$.

Following [68], let us introduce the first energy moment and the position of the energy center:

$$\mathbf{M} \stackrel{\text{def}}{=} \sum_{\mathbf{r}} \mathbf{r} \, \epsilon(\mathbf{r}), \quad \mathbf{r}_c \stackrel{\text{def}}{=} \frac{\mathbf{M}}{E}. \quad (6)$$

The vector $\mathbf{r}_c$ defines the center of the spatial energy distribution in the lattice. Definitions of $\mathbf{M}$ and $\mathbf{r}_c$ are analogous to the static moment and the center of mass, respectively, that are used in classical mechanics to describe the spatial distribution of massive particles. Therefore, here, $\mathbf{r}_c$ will be referred to as the center of energy or the energy center. In the present work, we limit our consideration to the disturbances for which the total energy (4) and the first energy moment (6) are finite.

Using differentiation of Eq. (6), we now introduce the total energy flux $\mathbf{h}$ and the energy transfer velocity $\mathbf{v}_c$ (the velocity of the energy center):

$$\mathbf{h} \stackrel{\text{def}}{=} \frac{d\mathbf{M}}{dt}, \quad \mathbf{v}_c \stackrel{\text{def}}{=} \frac{d\mathbf{r}_c}{dt} = \frac{\mathbf{h}}{E}. \tag{7}$$

From the last formula we have $\mathbf{h} = E\mathbf{v}_c$; hence, the total energy flux $\mathbf{h}$ describes the propagation of energy over the lattice in the same way that the total momentum describes the propagation of mass in space. Calculating the time derivative of $\mathbf{M}$ using Eqs. (1), (5), and (6) gives the following representation for the total energy flux:

$$\mathbf{h} = \frac{1}{2} \sum_{\mathbf{r}, \alpha} \mathbf{a}_\alpha \, C_\alpha \, u(\mathbf{r}) \, v(\mathbf{r} + \mathbf{a}_\alpha). \tag{8}$$

Further differentiation using (1) gives

$$\frac{d\mathbf{h}}{dt} = 0 \quad \Rightarrow \quad \mathbf{h} = \text{const}, \tag{9}$$

the conservation of the total energy flux in a simple harmonic scalar lattice. A detailed derivation of formulas (8) and (9) is given in Appendix A. From (9) it follows that the energy transfer velocity is conserved: $\mathbf{v}_c = \text{const}$. Then the position of the energy center at any moment of time is

$$\mathbf{r}_c = \overset{\circ}{\mathbf{r}}_c + \mathbf{v}_c t, \tag{10}$$

where $\overset{\circ}{\mathbf{r}}_c$ is the initial value of $\mathbf{r}_c$. Thus, the center of energy for any finite energy disturbance in a simple harmonic scalar lattice moves rectilinearly and uniformly. Here, we have a complete analogy with the motion of the center of mass of a free body in classical mechanics. Constants $\overset{\circ}{\mathbf{r}}_c$ and $\mathbf{v}_c$ in Eq. (10) are uniquely determined from the initial conditions by Eqs. (4)–(8). Explicit formulas for these vectors in the case of a square lattice are given in Appendix B.

C. Traveling waves

Equation (1) possesses a solution in the form of traveling harmonic waves,

$$u(\mathbf{r}) = U \sin(\boldsymbol{\kappa} \cdot \mathbf{r} - \omega t + \phi), \tag{11}$$

where U is the amplitude, $\boldsymbol{\kappa}$ is the wave vector, ω is the wave frequency, and ϕ is the phase shift. Substituting function (11) into the equation of motion (1) results in the dispersion relation $\omega = \omega(\boldsymbol{\kappa})$. The direction of the phase wave motion for Eq. (11) is defined by the wave vector $\boldsymbol{\kappa}$. However, it is generally accepted that the direction of energy propagation can be different since it is associated with the direction of the group velocity vector:

$$\mathbf{v}_g \stackrel{\text{def}}{=} \frac{d\omega}{d\boldsymbol{\kappa}}. \tag{12}$$

Solution (11) satisfies the following initial conditions:

$$\overset{\circ}{u}(\mathbf{r}) = U \sin(\boldsymbol{\kappa} \cdot \mathbf{r} + \phi), \quad \overset{\circ}{v}(\mathbf{r}) = -\omega U \cos(\boldsymbol{\kappa} \cdot \mathbf{r} + \phi), \tag{13}$$

where the circle accent denotes the initial values of the variables. To have a localized disturbance, the initial conditions (13) will be modified by replacing constant U by the following envelope function:

$$U(\mathbf{r}) \stackrel{\text{def}}{=} \gamma A \cos^{2k}\left(\frac{\pi r}{D}\right) \tag{14}$$

for $r \leqslant D/2$, and otherwise, $U(\mathbf{r}) = 0$. Here, $r \stackrel{\text{def}}{=} |\mathbf{r}|$, A is a constant amplitude, and γ is the dimensionless correction factor. The parameter k is the shape factor; it determines the shape of the envelope, which is cylindrical for $k = 0$ and bell shaped for $k = 1$. The value of the correction factor is chosen depending on k in order to have the same total energy for disturbances with different shapes.

The disturbance, defined by initial conditions (13) and (14), is localized in a circle of diameter D. The energy center of the disturbance should move with constant energy transfer velocity $\mathbf{v}_c$, defined by (7). This velocity can be obtained from initial conditions in view of conservation of the total energy and the total energy flux. On the other hand, the disturbance is supposed to move in the direction of the group velocity $\mathbf{v}_g$. Thus, we have the following questions, which are among the main issues of the current work:

(i) Is the group velocity $\mathbf{v}_g$ close to the velocity of the energy center $\mathbf{v}_c$, or can a noticeable difference be observed?

(ii) Can we describe the motion of the disturbance as a motion of a point mass in conventional mechanics?

(iii) Will the localization of the disturbance remain during its motion?

These questions will be studied below using computer simulations in the case of a square lattice.

III. SQUARE LATTICE

A. Wave vector and group velocity

1. Basic formulas

For the square lattice, function (11) satisfies the equation of motion (3) if the following dispersion relation holds:

$$\omega = 2\omega_e \sqrt{\sin^2 \frac{q_x}{2} + \sin^2 \frac{q_y}{2}}, \tag{15}$$

where $\omega_e \stackrel{\text{def}}{=} \sqrt{C/m}$ is the elementary frequency, $q_x = \mathbf{q} \cdot \mathbf{e}_1$ and $q_y = \mathbf{q} \cdot \mathbf{e}_2$ are the dimensionless wave numbers, $\mathbf{q} = a\boldsymbol{\kappa}$ is the dimensionless wave vector, and $\mathbf{e}_1$ and $\mathbf{e}_2$ are the unit vectors shown in Fig. 1. Relation (15) can be obtained by representing solution (11) in exponential form, $u(\mathbf{r}) = \text{Re}\,(Ze^{i(\boldsymbol{\kappa} \cdot \mathbf{r} - \omega t)})$, where Z is an appropriate complex constant and i is the imaginary unit. Then substitution of the exponent into Eq. (3) results in the dispersion relation, Eq. (15).

The group velocity vector (12) can be calculated as

$$\mathbf{v}_g = \frac{d\omega}{d\boldsymbol{\kappa}} = \frac{1}{a}\left(\frac{\partial \omega}{\partial q_x} \mathbf{e}_1 + \frac{\partial \omega}{\partial q_y} \mathbf{e}_2\right). \tag{16}$$

The corresponding derivatives using Eq. (15) give, for projections $v_{gx} = \mathbf{v}_g \cdot \mathbf{e}_1$ and $v_{gy} = \mathbf{v}_g \cdot \mathbf{e}_2$ of the group velocity, the
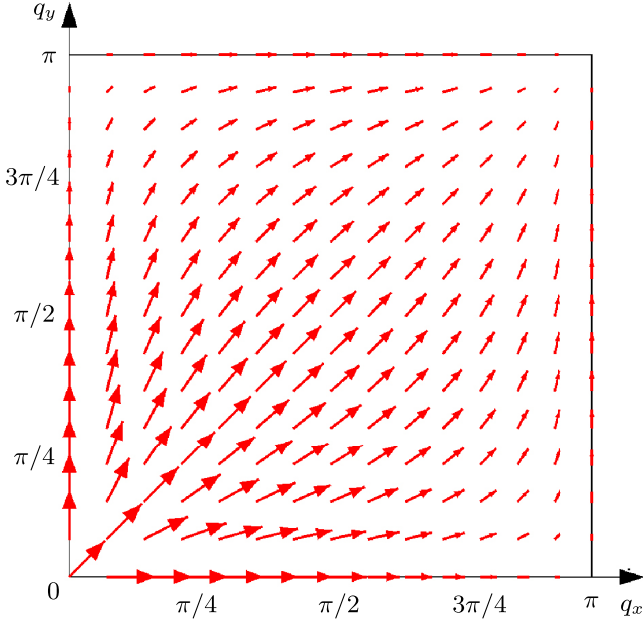
FIG. 2. Velocity vector field. The arrows indicate the magnitude and direction of the velocity vector.

FIG. 3. The energy center velocity as a function of the wave numbers.

following representations:

$$v_{gx} = \frac{c \sin q_x}{2\sqrt{\sin^2 \frac{q_x}{2} + \sin^2 \frac{q_y}{2}}}, \quad v_{gy} = \frac{c \sin q_y}{2\sqrt{\sin^2 \frac{q_x}{2} + \sin^2 \frac{q_y}{2}}}, \quad (17)$$

where $c \stackrel{\text{def}}{=} a\omega_e$ is the sound velocity, that is, the velocity of the infinitely long waves in the lattice. The modulus of the group velocity is

$$v_g \stackrel{\text{def}}{=} \sqrt{v_{gx}^2 + v_{gy}^2} = \frac{c}{2}\sqrt{\frac{\sin^2 q_x + \sin^2 q_y}{\sin^2 \frac{q_x}{2} + \sin^2 \frac{q_y}{2}}}. \quad (18)$$

It can be shown from Eq. (18) that $v_g \leqslant c$.

2. Vector field

The field of velocities, given by Eq. (17), is shown in Fig. 2. Red arrows indicate the magnitude and direction of the velocity vector as a function of the wave numbers.

As can be seen from Fig. 2, the magnitude of the velocity vectors decreases with the increase of the value of the wave vector. When q_x or q_y is equal to π, the velocity approaches zero, and we have a standing wave. Figure 2 elucidates that the direction of the group velocity coincides with the direction of the wave vector only in some particular cases. Let us introduce $q = |\mathbf{q}|$, $\mathbf{e} = \mathbf{q}/q$; then these particular cases can be represented as follows.

(i) For the bond direction, $q_x q_y = 0$, and then $\mathbf{v}_g = c \cos\left(\frac{q}{2}\right)\mathbf{e}$.

(ii) For the diagonal direction, $|q_x| = |q_y|$, and $\mathbf{v}_g = c \cos\left(\frac{q}{2\sqrt{2}}\right)\mathbf{e}$.

(iii) For long waves, $q \ll 1$, and then $\mathbf{v}_g \approx c\mathbf{e}$.

The codirection of the wave vector and the group velocity in the first two cases also follows from the symmetry: If the wave vector is directed along a symmetry axis of the lattice,
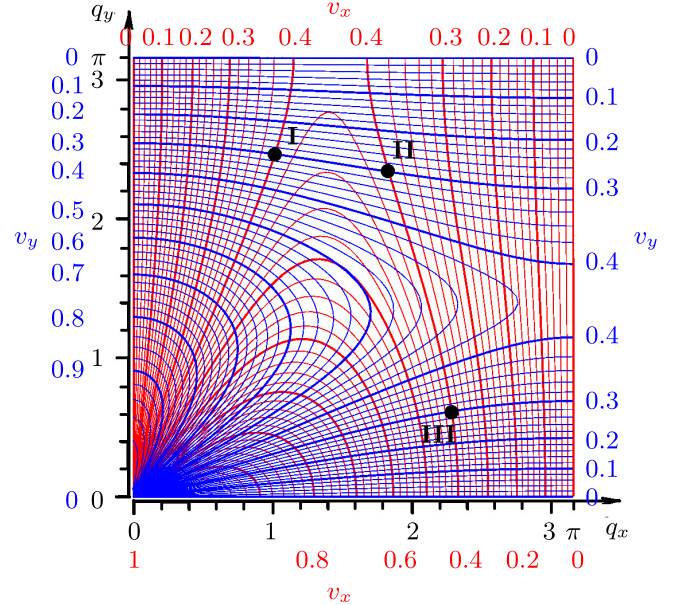
then any direction of the group velocity other than the axis direction breaks the symmetry of the system. In the third case, the codirection is due to the isotropy of the lattice for long waves (in this case the discreteness of the system can be neglected).

In cases other than those mentioned above, the directions of $\mathbf{q}$ and $\mathbf{v}_g$ are normally different: The symmetry reasons here are not applicable, and the lattice anisotropy is significant. The situation is similar to a sailboat driven by the wind (the analog of the wave vector) where the keel of the boat (the analog of the lattice axis) is directed differently: Then, the direction of the boat's motion (the analog of the group velocity) is different from both mentioned directions.

3. Inverse problem

Commonly, the wave numbers q_x and q_y are known, and the group velocity projections v_{gx} and v_{gy} can be calculated from Eq. (17). However, it can be useful, especially for computer modeling, to solve the inverse problem: Find the wave vector from the known value of the group velocity. This can be done numerically by calculating the relations $q_x = q_x(|v|, \varphi)$ and $q_y = q_y(|v|, \varphi)$, where $|v| = (v_{cx}^2 + v_{cy}^2)^{1/2}$ is the modulus of the velocity of the energy center and $\tan \varphi = v_{cy}/v_{cx}$. The result of the numeric solving of the inverse problem using the Wolfram's *Mathematica* software is presented in Fig. 3 in the form of a nomogram, where projections of the energy center velocities v_{cx} and v_{cy} can be found for any combination of wave numbers q_x and q_y. From the nomogram it can be deduced that inside the circle $q_x^2 + q_y^2 \leqslant (2\pi/3)^2$ there is a one-to-one relationship between $\mathbf{q}$ and $\mathbf{v}_g$. However, outside this circle, the dependence of the velocity projections on the wave numbers is multivalued. For example, from Fig. 3 one can see that velocity $(v_x, v_y) = (0.4, 0.3)$ can be obtained for three different sets of wave numbers (q_x, q_y),
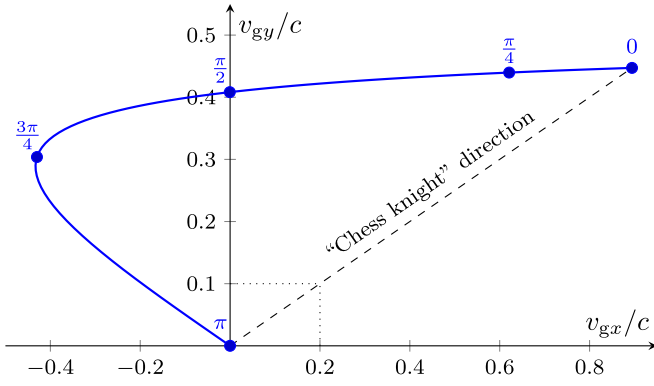
FIG. 4. Velocity hodograph for $q_x = 2q_y$ ("chess knight" direction). The numbers near nodes depict the values of q_y.

TABLE I. Parameters of the numerical experiments: q_x and q_y are the wave numbers, k is the shape factor of the initial disturbance, $\overline{D}$ is the dimensionless initial diameter of the disturbance, N is the dimensionless size of the simulation cell, and $\bar{t}_{\max}$ is the dimensionless integration time. Here, "var" indicates parameters taking a range of values.

Fig.	q_x	q_y	k	$\overline{D}$	N	$\bar{t}_{\max}$
5	$\pi/8$	0	1	100	1000	0
6	$\pi/4$	0	var	200	2000	400
8	var	0	1	100	2000	var
7	var	0	1	100	1200	700
9	var	var	1	100	1000	400
10	var	var	1	200	2000	2500

marked by points I–III: I, (1.00, 2.50); II, (1.84, 2.35); and III, (2.28, 0.64).

4. Hodograph

As an example, when the wave vector and the group velocity are not codirected, we consider the "chess knight" direction of the wave vector, $q_x = 2q_y$, which follows the path taken by the knight playing piece in chess. The hodograph for the group velocity in this case is shown in Fig. 4. The hodograph curve follows the tip of the group velocity vector for various values of q_y. Figure 4 demonstrates that the directions of $\mathbf{q}$ and $\mathbf{v}_g$ coincide only for small q_y; for other values of q_y the directions are surprisingly different. More complex hodographs can be obtained for other values of q_y/q_x, especially if this ratio is irrational.

B. Simulation technique

We consider a square mesh of $N \times N$ particles with periodic boundary conditions. The initial disturbance for the particles is set using initial conditions (13) and (14) inside a circle of diameter D, while all other particles have zero displacements and velocities. To minimize boundary effects, in all experiments we keep the relation $D \leqslant 0.1Na$.

Let us introduce the following dimensionless time and space coordinates:

$$\bar{t} \stackrel{\text{def}}{=} \omega_e t, \quad \bar{x} \stackrel{\text{def}}{=} x/a = i, \quad \bar{y} \stackrel{\text{def}}{=} y/a = j. \quad (19)$$

The main parameters for the numeric experiments are the size of the simulation cell $N \times N$, the shape factor of the disturbance k, the wave vectors q_x and q_y, the initial dimensionless diameter of the disturbance $\bar{D} = D/a$, and the maximum integration time $\bar{t}_{\max}$. Table I shows the values of these parameters used in each case under consideration. The parameters that take a range of values are marked as "var."

In Figs. 5(a)–5(d), the distribution of the local energy, displacement, and velocity for a typical initial disturbance is shown. The wave numbers are $q_x = \pi/8$ and $q_y = 0$ (for other parameters see Table I). The disturbance is excited in a bell-shaped form ($k = 1$). We consider three main characteristics of the disturbance: The local energy ϵ (as the ratio to the maximum energy $\epsilon_{\max}$), the value of the displacements u for each particle in the disturbance (as the ratio to the maximum

displacement $u_{\max}$), and velocities for each particle in the disturbance (as the ratio to the maximum velocity $v_{\max}$). Figure 5(d) demonstrates a perspective view of the disturbance in terms of energy and spatial coordinates. Note that the ratio of a quantity to its maximum value is the same in both dimensional and dimensionless forms.

A weak reverse-wave effect is observed when using the initial conditions (13) and (14): Simultaneously with the main disturbance moving in the forward direction, an additional disturbance with much lower energy moving in the opposite direction is realized. To minimize this effect, the following method is used: The initial displacements and velocities (13) are multiplied by constant coefficients, so that the initial po-
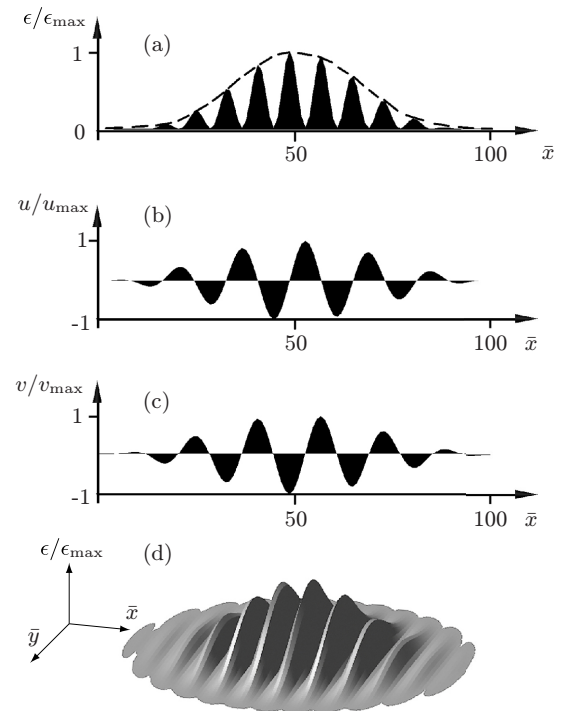

FIG. 5. (a) Local energy, (b) displacement, and (c) velocity of the disturbance, shown as functions of the dimensionless spatial coordinate $\bar{x}$, and (d) a perspective view of the initial disturbance. The maximum values of the local energy, displacement, and velocity are indicated by "max."
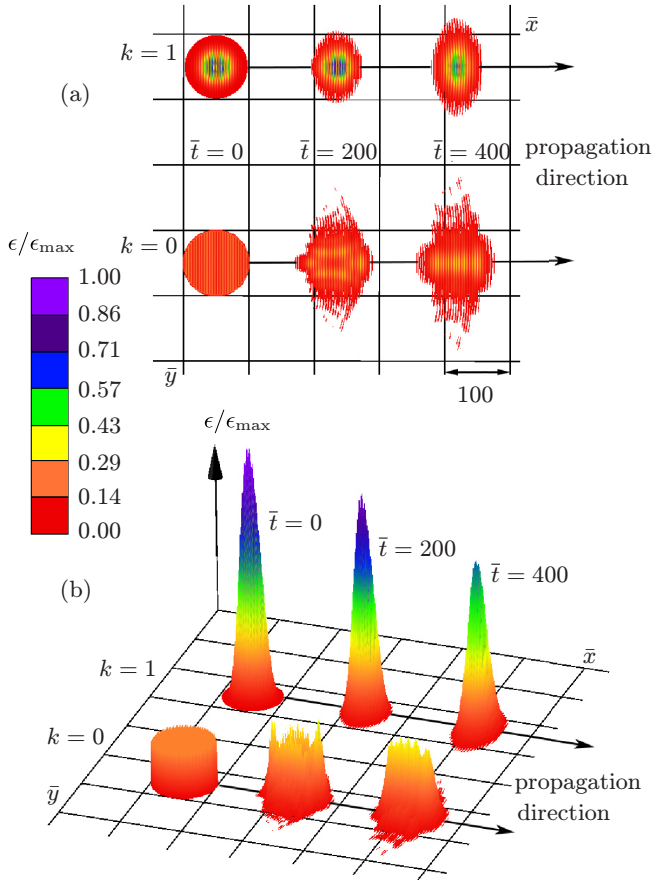
FIG. 6. Evolution of the energy distribution during propagation of the disturbance with the shape factors $k = 0$ and $k = 1$ (a) as a projection to the lattice plane and (b) in a perspective representation. The propagation direction is shown by arrows. The other parameters are shown in Table I. $\epsilon_{\max}$ is the maximum local energy for the initial bell-shaped disturbance.

tential and kinetic energy become equal to half of the total energy (these coefficients are always close to 1). After such a change in the initial conditions, the reverse wave becomes insignificant and therefore not visible in the figures.

The details of the numeric integration method are given in Appendix C.

C. Motion of a single disturbance

1. Shape factor and disturbance evolution

We study two different shapes of the disturbance (14): Cylindrical ($k = 0$) and bell shaped ($k = 1$). The evolution of the energy distribution during its propagation is shown in Fig. 6 as a projection on the lattice plane [Fig. 6(a)] and in a perspective view [Fig. 6(b)]. Table I gives the parameters used for the case under consideration. To make the total energy for both disturbances the same, we set a correction factor in Eq. (14), $\gamma = 0.45$ for $k = 0$ and $\gamma = 1$ for $k = 1$.

As can be seen from Fig. 6, the energy centers for both types of disturbances propagate rectilinearly and uniformly. At the initial moment, the projection on the lattice plane for both disturbances has circular symmetry. At $\bar{t} = 400$, for the cylindrical type of disturbance ($k = 0$), the projection on the
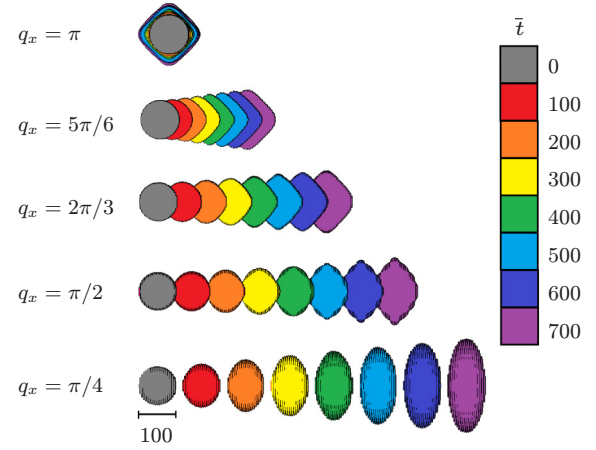

FIG. 7. Motion of disturbances with various wave numbers q_x.

lattice plane transforms to a trilobite-like shape, while for the bell-shaped function ($k = 1$) the disturbance possesses an elliptical shape. This difference is due to the smoothness of the bell-shaped function. Figure 6(b) shows that the initial disturbances in both cases propagate for a distance at least 5 times greater than the diameter of the initial disturbance without significant energy dispersion. This demonstrates a high stability of the disturbance. Further, only the bell-shaped disturbances will be considered.

2. Motion and dispersion of the disturbance

In Fig. 7, the motion of the bell-shaped disturbance along the bond direction for different wave numbers q_x is presented as a projection to the lattice plane. The parameters are listed in Table I. For better visualization, the projection of the disturbance at each moment of time is marked by the corresponding color. A decrease in the wave number (an increase in the wavelength) results in an increase in $\mathbf{v}_c$, which is clearly seen in Fig. 7. A clot of energy, associated with the disturbance, moves similarly to a free body of matter in classical mechanics: For any value of q_x, it propagates rectilinearly and uniformly. For $q_x = \pi$ we obtain a standing wave: $\mathbf{v}_c = 0$. It can be seen from Fig. 7, that the disturbance projection transforms from circular to rhombic ($q_x > \pi/2$) or elliptic ($q_x < \pi/2$). Thus, the energy dispersion is anisotropic: At a higher velocity, the disturbance acquires a flattened shape in the direction of its motion.

3. Group velocity and energy center velocity

To confirm the possibility to describe the propagation of the disturbance in terms of the kinetic model, we need to compare the values of the energy center velocity $\mathbf{v}_c$ (7) and the group velocity $\mathbf{v}_g$ (12). Such a comparison is presented in Fig. 8 for the square lattice; the corresponding parameters are shown in Table I. The group velocity (the black upper line) is calculated from Eq. (17); therefore, it characterizes only the delocalized harmonic wave process (11) and does not take into account the peculiarities of the shape function. On contrary, the energy center velocity can be calculated only for a localized disturbance; therefore, the shape function here is essential. We calculate the energy center velocity using two
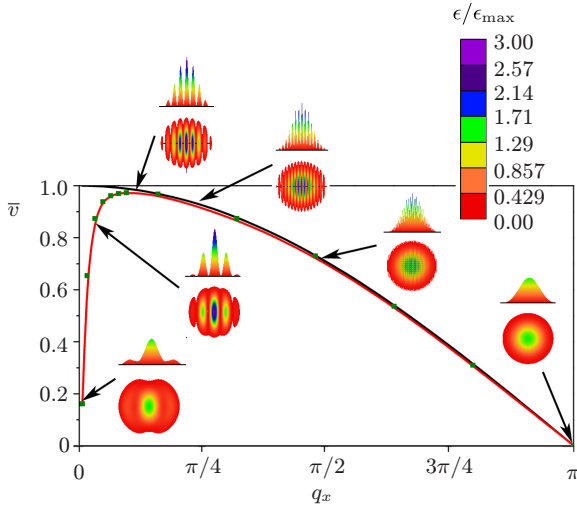
FIG. 8. Velocity of the energy clot as a function of wave number q_x. The black upper line corresponds to the group velocity $\mathbf{v}_g$ analytically obtained from Eq. (17), the red line corresponds to the numerical calculations of the actual value of the energy center velocity $\mathbf{v}_c$, and the green squares correspond to the initial value of $\mathbf{v}_c$. The disturbance is plotted as an energy profile and a projection to the lattice plane. Here, ϵ_{max} is the maximum local energy for the case $q_x = \pi/10$.

methods. One method (the green squares) calculates the initial value of the velocity using Eq. (B2). Another method (the red line) calculates the energy center position using Eq. (B1) in the process of the computer simulations, and the actual velocity is obtained numerically from the change in the energy center location. We also show in Fig. 8 the energy distribution as an energy profile and as a projection to the lattice plane. The parameters are shown in Table I.

From Fig. 8 it follows that the energy center velocities $\mathbf{v}_c$ calculated using both methods (the red line and green squares) are almost indistinguishable in the scale of the graph. The group velocity $\mathbf{v}_g$ (the black upper line) coincides well only with the decreasing part of the $\mathbf{v}_c$ dependence on the wave number. The increasing part of the dependence, observed when the wavelength of the initial disturbance is close to its diameter ($q_x < \pi/10$), has no correlation with the values of $\mathbf{v}_g$. Thus, if at least several periods of the harmonic wave process (11) can be fitted in the initial diameter D, $\mathbf{v}_g$ and $\mathbf{v}_c$ are in good correlation, and such disturbances can be used in kinetic models as models of phonons. Otherwise, a notable deviation should be expected, which should be taken into account when dynamic and kinetic models are compared.

D. Motion of several disturbances

Figure 9 shows the motion of three energy clots that have emerged from the same starting position. The parameters are presented in Table I. The initial disturbance is a superposition of three disturbances having the same total energy and equal absolute value as the energy center velocity ($\bar{v} = 0.9$). The directions of the energy center velocities are different; we choose the following as an example: Bond direction ($\bar{v}_x = 0$), diagonal direction ($\bar{v}_x = \bar{v}_y$), and chess-knight
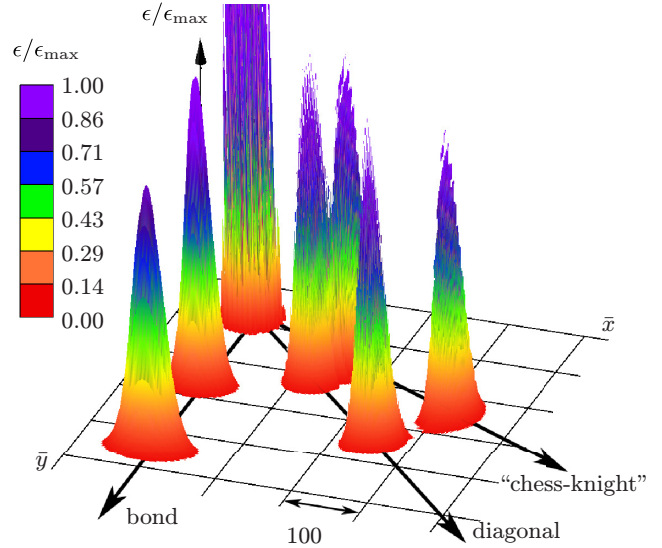
direction ($\bar{v}_x = 2\bar{v}_y$). The corresponding wave numbers (q_x, q_y) are $(2\pi/7, 0)$, $(2\pi/7, 2\pi/7)$, and $(2\pi/15, \pi/3)$. Figure 9 demonstrates the resulting energy distribution in the lattice at three moments in time: $\bar{t} = 0$, 200, and 400 (the initial peak is partially shown). As can be seen, each disturbance moves rectilinearly and uniformly; the energy dispersion is not significant when the disturbances pass several of their initial diameters.

In Fig. 10 the energy distribution during the motion of two disturbances initially placed at sites A_1 and A_2 is presented. The corresponding wave numbers (q_x, q_y) are $(\pi/7, 2\pi/3)$ and $(\pi/7, 9\pi/7)$; for other parameters, see Table I. Short arrows show the motion direction step by step from point A_1 to E_1 for the first energy disturbance and from point A_2 to E_2 for the second one. The energy distributions are visualized at $\bar{t} = 0$, 400, 800, 1200, and 1600. As we can see from Fig. 10,
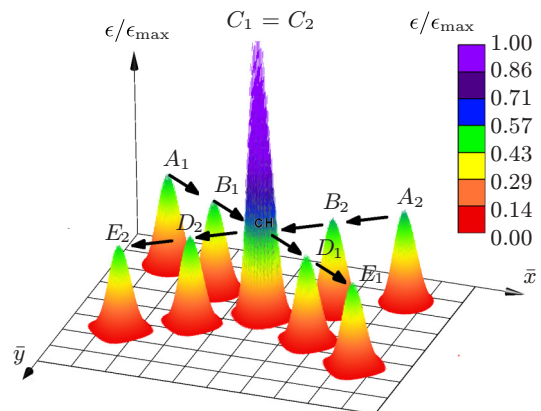

FIG. 9. Evolution of the energy distribution for the simultaneous motion of three energy clots obtained from a superposed initial disturbance; ϵ_{max} is the maximum local energy for the individual initial disturbances. Bold arrows show the motion directions.

FIG. 10. Motion of the disturbances: Arrows show the motion directions for $\bar{t} = 0$ (A_1, A_2), 400 (B_1, B_2), 800 ($C_1 = C_2$), 1200 (D_1, D_2) and 1600 (E_1, E_2); ϵ_{max} is the maximum local energy at $C_1 = C_2$.

both energy disturbances propagate uniformly, each with a constant velocity ($\bar{v} = 0.5$). At $\bar{t} = 800$ ($C_1 = C_2$) the energy clots join, forming a greater energy clot with a maximum that is far more than 2 times higher than for the individual disturbances. This is due to the fact that, although the system is linear, the energy is not additive (being a quadratic function of velocities and displacements). After point $C_1 = C_2$ the disturbances separate without any changes in propagation direction and without significant energy dispersion. This example demonstrates the high stability of the disturbances and their opportunity to conserve their velocities and shapes after "collisions." Since the system is harmonic, there are no true collisions—we simply have a superposition of two solutions. However, low dispersion for the considered solutions allows us to observe the motion of the energy clots in analogy to the motion of point masses in the conventional mechanics of particles.

IV. DISCUSSION AND CONCLUDING REMARKS

We have analytically and numerically studied energy transfer in scalar harmonic lattices. Using the first moment of the energy distribution, the notions of the energy center and the total energy flux were introduced for localized disturbances. It was proved analytically (for an arbitrary infinite simple harmonic scalar lattice) and confirmed numerically (for a square lattice) that the total energy flux is conserved and the energy center moves rectilinearly and uniformly, mimicking the momentum and the center of mass of a set of free particles in conventional mechanics. We applied the methods for energy dynamics, introduced for one-dimensional systems in [68], to multidimensional discrete systems. The obtained results confirmed the validity of energy dynamics for the case of energy transfer in many directions. Although the considered processes correspond to energy kinematics rather than dynamics (the crystal is uniform and harmonic; therefore, the disturbances move as free particles, and no energy forces are applied to them), the processes under consideration are important for understanding energy transfer in lattice systems and establish a link between the lattice dynamics and the phonon kinetics.

Moving localized disturbances can be observed in various elastic systems. In particular, they can be found as exact solutions for continuous media, where the equations of dynamics can be reduced to the wave equation in one, two, and three dimensions, e.g., localized electromagnetic and acoustic waves [24,69–71]. In the present paper, such localized solutions are obtained numerically for a discrete medium that is a scalar crystal lattice. We suggested a special form of the initial disturbance, a harmonic wave with variable amplitude, given by a shape function. Due to conservation of the total energy flux, which was proved, the energy centers of the localized disturbances move uniformly, and this appears to be an important and representative feature of scalar lattices. An energy clot associated with such a disturbance moves without significant dispersion, which allows us to consider it a quasiparticle.

For the square lattice, we analyzed the correlation between the directions of the wave vector and the group velocity, and three cases in which these vectors coincide were distinguished. Then the vectors of the group velocity and the energy center velocity were compared for different values of the wave vector. It was shown that for the disturbances containing at least several periods of the harmonic wave, these two velocities are almost equal. Thus, such disturbances can be used in kinetic models as prototypes of phonons. If the length of the harmonic wave is close to the initial diameter of the disturbance, notable deviations are observed, which should be taken into account when dynamic and kinetic models are compared. It was shown that in the case of several localized disturbances they pass through each other and move continuously, conserving their velocities without significant energy dispersion, allowing us to observe the motion of the corresponding energy clots, in analogy to the motion of point masses in the conventional mechanics of particles.

Further extensions of the model under consideration can be associated with two main features of real lattices: Anharmonicity and imperfection. In part, these issues were studied for one dimension in [68], where the method of energy dynamics was applied, in particular, for anharmonic and imperfect systems. Extending these results to the current 2D case, we can conclude that similar effects can be expected. First, for the anharmonic case, the interaction of the disturbance with the carrier will be observed. This interaction can affect the disturbance propagation and, in particular, change the velocity of its energy center. However, in some cases, the energy center can move uniformly even in the anharmonic case, as solitons do [54,56]. Another important effect of anharmonicity is the mutual interaction of disturbances; such interaction is essential for the kinetics of collisional phonons [11,48,56]. Second, the lattice imperfection will affect the disturbance motion even more than anharmonicity. Indeed, any imperfection produces a quasiforce, which causes the energy center of the disturbance to move in the same way as a massive particle moves in a force field in accordance with Newton's second law [68]. A gradual change in the properties of the lattice can cause effects on the motion of the energy center similar to those studied in gradient-index optics [72–74]. All these effects are undoubtedly important, but they require additional research, which is beyond the scope of this paper. However, if the anharmonicity is small and imperfections are rare, the results of this paper can be used as a first approximation, which can then be improved using a perturbation method. Moreover, the exact integral of the energy flux and the constancy of the velocity of the energy center obtained in this study provide the necessary basis for the analysis of more complex systems.

APPENDIX A: ENERGY FLUX

Let us derive (8), which represents the total energy flux in terms of displacements and velocities. Consider the equation of motion (1) and the formula for the local energy (5) in

the form

$$m\dot{v} = \sum_\alpha C_\alpha(u_\alpha - u), \quad \epsilon = \frac{m}{2}v^2 + \sum_\alpha \frac{C_\alpha}{4}(u_\alpha - u)^2,$$

(A1)

where the overdot stands for the time derivative, u_α is a short form of $u(\mathbf{r} + \mathbf{a}_\alpha)$, and the dependence of the variables on $\mathbf{r}$ is omitted for simplicity. Differentiation of the local energy with the use of the equation of motion gives

$$\dot{\epsilon} = \frac{1}{2}\sum_\alpha C_\alpha(v_\alpha + v)(u_\alpha - u).$$

(A2)

Then, according to Eqs. (6) and (7), for the total energy flux we have

$$\mathbf{h} = \sum_\mathbf{r} \mathbf{r}\,\dot{\epsilon} = \frac{1}{2}\sum_{\mathbf{r},\alpha}\mathbf{r}\,C_\alpha(v_\alpha + v)(u_\alpha - u).$$

(A3)

The lattice possesses central symmetry (invariance in changing from α to $-\alpha$); hence, the above formula can be rewritten as

$$\mathbf{h} = \frac{1}{2}\sum_{\mathbf{r},\alpha}\mathbf{r}\,C_\alpha(v_{-\alpha} + v)(u_{-\alpha} - u),$$

(A4)

where $u_{-\alpha} = u(\mathbf{r} + \mathbf{a}_{-\alpha}) = u(\mathbf{r} - \mathbf{a}_\alpha)$. The lattice is shift invariant; therefore, in the above sum we can change $\mathbf{r}$ to $\mathbf{r} + \mathbf{a}_\alpha$, which changes u to u_α, $u_{-\alpha}$ to u, etc. Then we have

$$\mathbf{h} = \frac{1}{2}\sum_{\mathbf{r},\alpha}(\mathbf{r} + \mathbf{a}_\alpha)\,C_\alpha(v + v_\alpha)(u - u_\alpha).$$

(A5)

Half the sum of Eqs. (A3) and (A5) gives

$$\mathbf{h} = \frac{1}{4}\sum_{\mathbf{r},\alpha}\mathbf{a}_\alpha\,C_\alpha(v + v_\alpha)(u - u_\alpha).$$

(A6)

Using the above-mentioned properties of the lattice symmetry (central symmetry and shift invariance), it can be easily proved that

$$\sum_{\mathbf{r},\alpha}\mathbf{a}_\alpha C_\alpha vu = \sum_{\mathbf{r},\alpha}\mathbf{a}_\alpha C_\alpha v_\alpha u_\alpha = 0.$$

(A7)

Then, we finally get the desired representation (8) for the total energy flux:

$$\mathbf{h} = -\frac{1}{2}\sum_{\mathbf{r},\alpha}\mathbf{a}_\alpha C_\alpha vu_\alpha = \frac{1}{2}\sum_{\mathbf{r},\alpha}\mathbf{a}_\alpha C_\alpha v_\alpha u.$$

(A8)

Now let us prove the conservation of the total energy flux (9). Time differentiation of the first equation in Eq. (A8) gives

$$\dot{\mathbf{h}} = -\frac{1}{2}\sum_{\mathbf{r},\alpha}\mathbf{a}_\alpha C_\alpha \dot{v}u_\alpha - \frac{1}{2}\sum_{\mathbf{r},\alpha}\mathbf{a}_\alpha C_\alpha vv_\alpha.$$

(A9)

From the lattice symmetry it follows that the second sum is zero. Then substitution of $\dot{v}$ from Eq. (A1) (where α is changed to β) gives

$$\dot{\mathbf{h}} = -\frac{1}{2m}\sum_{\mathbf{r},\alpha,\beta}\mathbf{a}_\alpha C_\alpha C_\beta\,(u_\beta - u)\,u_\alpha,$$

(A10)

and after reduction for symmetry reasons

$$\dot{\mathbf{h}} = -\frac{1}{2m}\sum_{\mathbf{r},\alpha,\beta}\mathbf{a}_\alpha C_\alpha C_\beta u_\beta u_\alpha.$$

(A11)

Changing α to $-\alpha$ and β to $-\beta$ yields

$$\dot{\mathbf{h}} = \frac{1}{2m}\sum_{\mathbf{r},\alpha,\beta}\mathbf{a}_\alpha C_{-\alpha}C_{-\beta}\,u_{-\beta}\,u_{-\alpha}.$$

(A12)

Shifting from $\mathbf{r}$ to $\mathbf{r} + \mathbf{a}_\alpha + \mathbf{a}_\beta$ changes $u_{-\beta}$ to u_α and $u_{-\alpha}$ to u_β; then Eq. (A12) takes the form

$$\dot{\mathbf{h}} = \frac{1}{2m}\sum_{\mathbf{r},\alpha,\beta}\mathbf{a}_\alpha C_\alpha C_\beta u_\beta u_\alpha.$$

(A13)

Half the sum of Eqs. (A11) and (A13) finally gives $\dot{\mathbf{h}} = 0$. Thus, we have strictly proved the conservation of the total energy flux for simple harmonic scalar lattices.

APPENDIX B: ENERGY CENTER POSITION AND VELOCITY FOR A SQUARE LATTICE

Here, we adopt formulas from Sec. II for the case of a square lattice. Some additional transformations are performed in order to make them more convenient for numerical calculations.

The energy center coordinates from Eqs. (5) and (6) are

$$x_c = \frac{ma}{2E}\sum_{i,j}iv_{i,j}^2 + \frac{Ca}{2E}\sum_{i,j}\left(i + \frac{1}{2}\right)(u_{i+1,j} - u_{i,j})^2$$
$$+ \frac{Ca}{2E}\sum_{i,j}i(u_{i,j+1} - u_{i,j})^2,$$

$$y_c = \frac{ma}{2E}\sum_{i,j}jv_{i,j}^2 + \frac{Ca}{2E}\sum_{i,j}j(u_{i+1,j} - u_{i,j})^2$$
$$+ \frac{Ca}{2E}\sum_{i,j}\left(j + \frac{1}{2}\right)(u_{i,j+1} - u_{i,j})^2.$$

(B1)

The energy center velocities from Eqs. (7) and (8) are

$$v_{cx} = \frac{Ca}{2E}\sum_{i,j}v_{i,j}(u_{i-1,j} - u_{i+1,j}),$$

$$v_{cy} = \frac{Ca}{2E}\sum_{i,j}v_{i,j}(u_{i,j-1} - u_{i,j+1}).$$

(B2)

The constant E in the above formulas is (4):

$$E = \frac{m}{2}\sum_{i,j}v_{i,j}^2 + \frac{C}{2}\sum_{i,j}(u_{i+1,j} - u_{i,j})^2$$
$$+ \frac{C}{2}\sum_{i,j}(u_{i,j+1} - u_{i,j})^2.$$

(B3)

The summation is performed for all $i = 1, 2, \ldots, N$ and $j = 1, 2, \ldots, N$. Since $\mathbf{v}_c$ and E are constants, the initial values of the particle displacements and velocities can be used in formulas (B2) and (B3).

The motion of the center of energy is described by vector formula (10),

$$\mathbf{r}_c = \overset{\circ}{\mathbf{r}}_c + \mathbf{v}_c t,$$

which in the coordinate form reads

$$x_c = \overset{\circ}{x}_c + v_{cx}t, \quad y_c = \overset{\circ}{y}_c + v_{cy}t.$$

The constants in the above formulas can be expressed in terms of initial conditions using Eqs. (B1)–(B3).

APPENDIX C: NUMERIC INTEGRATION SCHEME

Let us introduce the following units of dimensions:

$$[t] = \omega_e^{-1}, \quad [\omega] = \omega_e, \quad [u] = a,$$

$$[v] = a\omega_e = c, \quad [E] = mc^2. \tag{C1}$$

Then, the dimensionless quantities can be defined:

$$\bar{t} = t/[t], \quad \bar{u}_{i,j} = u_{i,j}/[u], \quad \bar{v}_{i,j} = v_{i,j}/[v],$$

$$\overline{U} = U/[u], \quad \overline{\omega} = \omega/[\omega], \quad \bar{\epsilon}_{i,j} = \epsilon_{i,j}/[E],$$

$$barx = x/[u] = i, \quad \bar{y} = y/[u] = j. \tag{C2}$$

Using Eqs. (C1) and (C2), we can rewrite Eq. (3) in the following dimensionless form:

$$\frac{d^2\bar{u}_{i,j}}{d\bar{t}^2} = \bar{u}_{i+1,j} + \bar{u}_{i-1,j} + \bar{u}_{i,j+1} + \bar{u}_{i,j-1} - 4\bar{u}_{i,j}. \tag{C3}$$

Initial conditions (13) using Eq. (C2) and $\phi = 0$ take the form

$$\overset{\circ}{\bar{u}}_{i,j} = \overline{U} \sin(q_x i + q_y j), \quad \overset{\circ}{\bar{v}}_{i,j} = -\overline{U}\overline{\omega} \cos(q_x i + q_y j). \tag{C4}$$

The local energy ϵ, which is defined by Eq. (5), can be rewritten as

$$\bar{\epsilon}_{i,j} = \frac{\bar{v}_{i,j}^2}{2} + \frac{(\bar{u}_{i,j+1} - \bar{u}_{i,j})^2 + (\bar{u}_{i,j-1} - \bar{u}_{i,j})^2}{4}$$

$$+ \frac{(\bar{u}_{i+1,j} - \bar{u}_{i,j})^2 + (\bar{u}_{i-1,j} - \bar{u}_{i,j})^2}{4}. \tag{C5}$$

To solve Eq. (C3) numerically, we use the method of central differences:

$$\bar{v}_{i,j}^{(n+1)} = \bar{v}_{i,j}^{(n)} + \bar{w}_{i,j}^{(n)}\Delta\bar{t}, \quad \bar{u}_{i,j}^{(n+1)} = \bar{u}_{i,j}^{(n)} + \bar{v}_{i,j}^{(n+1)}\Delta\bar{t}, \tag{C6}$$

where

$$\bar{w}_{i,j}^{(n)} = \bar{u}_{i+1,j}^{(n)} + \bar{u}_{i,j+1}^{(n)} + \bar{u}_{i-1,j}^{(n)} + \bar{u}_{i,j-1}^{(n)} - 4\bar{u}_{i,j}^{(n)} \tag{C7}$$

is the dimensionless acceleration, n is the time iteration number, and $\Delta\bar{t}$ is the dimensionless time step, which is less than or equal to 0.1.

[1] C. S. Coffey and S. J. Jacobs, Detection of local heating in impact or shock experiments with thermally sensitive films, J. Appl. Phys. **52**, 6991 (1981).

[2] D. D. Dlott and M. D. Fayer, Shocked molecular solids: Vibrational up pumping, defect hot spot formation, and the onset of chemistry, J. Chem. Phys. **92**, 3798 (1990).

[3] S. Ye, K. Tonokura, and M. Koshi, Energy transfer rates and impact sensitivities of crystalline explosives, Combust. Flame **132**, 240 (2003).

[4] M. Kaviany, *Heat Transfer Physics*, 2nd ed. (Cambridge University Press, New York, 2014).

[5] Y. Guo and M. Wang, Phonon hydrodynamics and its applications in nanoscale heat transport, Phys. Rep. **595**, 1 (2015).

[6] R. Saito, M. Mizuno, and M. S. Dresselhaus, Ballistic and Diffusive Thermal Conductivity of Graphene, Phys. Rev. Appl. **9**, 024017 (2018).

[7] V. A. Kuzkin and A. M. Krivtsov, Unsteady ballistic heat transport: Linking lattice dynamics and kinetic theory, Acta Mech. **232**, 1983 (2021).

[8] C. M. Lawson, E. E. Freed, and R. C. Powell, Models for energy transfer in solids. II, J. Chem. Phys. **76**, 4171 (1982).

[9] A. V. Savin and Y. A. Kosevich, Conformations and thermal dynamics of graphene-based polymer nanocarpets, Mater. Sci. Eng., B **264**, 114920 (2021).

[10] J. A. Baimova, R. T. Murzaev, and A. I. Rudskoy, Discrete breathers in graphane in thermal equilibrium, Phys. Lett. A **381**, 3049 (2017).

[11] D. G. Cahill, W. K. Ford, K. E. Goodson, G. D. Mahan, A. Majumdar, H. J. Maris, R. Merlin, and S. R. Phillpot, Nanoscale thermal transport, J. Appl. Phys. **93**, 793 (2003).

[12] W. G. Hoover and C. G. Hoover, Nonequilibrium temperature and thermometry in heat-conducting ϕ^4 models, Phys. Rev. E **77**, 041104 (2008).

[13] A. M. Krivtsov, Energy oscillations in a one-dimensional crystal, Dokl. Phys. **59**, 427 (2014).

[14] A. M. Krivtsov, Heat transfer in infinite harmonic one-dimensional crystals, Dokl. Phys. **60**, 407 (2015).

[15] O. V. Gendelman and J. Paul, Kapitza thermal resistance in linear and nonlinear chain models: Isotopic defect, Phys. Rev. E **103**, 052113 (2021).

[16] M. Gzal, B. Fang, A. F. Vakakis, L. A. Bergman, and O. V. Gendelman, Rapid non-resonant intermodal targeted energy transfer (IMTET) caused by vibro-impact nonlinearity, Nonlinear Dyn. **101**, 2087 (2020).

[17] E. M. Purcell and D. J. Morin, *Electricity and Magnetism*, 3rd ed. (Cambridge University Press, Cambridge, 2013).

[18] S. V. Bondarchuk, Theory of impact sensitivity revisited: Mechanical-to-vibrational energy transfer phenomenon, FirePhysChem. **2**, 334 (2022).

[19] A. F. Vakakis, O. V. Gendelman, L. A. Bergman, A. Mojahed, and M. Gzal, Nonlinear targeted energy transfer: State of the art and new perspectives, Nonlinear Dyn. **108**, 711 (2022).

[20] J. D. Achenbach, *Wave Propagation in Elastic Solids*, North Holland Series in Applied Mathematics and Mechanics Vol. 16 (North-Holland, Amsterdam, 1973).

[21] G. B. Whitham, *Linear and Nonlinear Waves* (Wiley, London, 1974).

[22] J. D. Jackson, *Classical Electrodynamics*, 3rd ed. (Wiley, New York, 1998).

[23] N. Morozov and Y. Petrov, *Dynamics of Fracture*, Foundation of Engineering Mechanics (Springer, Berlin, 2000).

[24] N. Kiselev, Localized light waves: Paraxial and exact solutions of the wave equation (a review), Opt. Spectrosc. **102**, 603 (2007).

[25] D. A. Indeitsev, V. N. Naumov, B. N. Semenov, and A. K. Belyaev, Thermoelastic waves in a continuum with complex structure, Z. Angew. Math. Mech. **89**, 279 (2009).

[26] V. M. Babich and A. P. Kiselev, *Elastic Waves: High Frequency Theory* (CRC Press, Boca Raton, FL, 2018).

[27] M. Gzal, A. F. Vakakis, L. A. Bergman, and O. V. Gendelman, Extreme intermodal energy transfers through vibro-impacts for highly effective and rapid blast mitigation, Numer. Simul. **103**, 106012 (2021).

[28] M. Kovaleva, V. Smirnov, and L. Manevitch, Nonstationary dynamics of the sine lattice consisting of three pendula (trimer), Phys. Rev. E **99**, 012209 (2019).

[29] C. Maradiya, J. Vadher, and R. Agarwal, The heat transfer enhancement techniques and their thermal performance factor, Beni-Suef Univ. J. Basic Appl. Sci. **7**, 1 (2018).

[30] L. Liu, J. Deng, D. Zhang, C. Wang, S. Qiu, and G. Su, Experimental analysis of flow and convective heat transfer in the water-cooled packed pebble bed nuclear reactor core, Prog. Nucl. Energy **122**, 103298 (2020).

[31] P. Xiong, Z. Qiu, Q. Lu, T. Lu, J. Deng, Y. Liu, and Y. Zhang, Simultaneous estimation of fluid temperature and convective heat transfer coefficient by sequential function specification method, Prog. Nucl. Energy **131**, 103588 (2021).

[32] Z. Rieder, J. L. Lebowitz, and E. Lieb, Properties of a harmonic crystal in a stationary nonequilibrium state, J. Math. Phys. **8**, 1073 (1967).

[33] F. Bonetto, J. L. Lebowitz, and L. Rey-Bellet, Fourier's law: A challenge to theorists, in *Mathematical Physics*, edited by A. Fokas, A. Grigorian, T. Kibble, B. Zegarlinski *et al.* (Imperial College Press, London, 2000).

[34] A. Dhar, Heat transport in low-dimensional systems, Adv. Phys. **57**, 457 (2008).

[35] O. Gendelman and A. Savin, Normal heat conductivity in chains capable of dissociation, Europhys. Lett. **106**, 34004 (2014).

[36] H. Spohn, Nonlinear fluctuating hydrodynamics for anharmonic chains, J. Stat. Phys. **154**, 1191 (2014).

[37] *Thermal Transport in Low Dimensions*, edited by S. Lepri, Lecture Notes in Physics Vol. 921 (Springer, Cham, 2016), p. 411.

[38] M. A. Guzev, The exact formula for the temperature of a one-dimensional crystal, Dal'nevost. Mat. Zh. **18**, 39 (2018).

[39] A. Dhar, A. Kundu, and A. Kundu, Anomalous heat transport in one dimensional systems: A description using non-local fractional-type diffusion equation, Front. Phys. **7**, 159 (2019).

[40] G. Benenti, S. Lepri, and R. Livi, Anomalous heat transport in classical many-body systems: Overview and perspectives, Front. Phys. **8**, 292 (2020).

[41] P. Desmarchelier, A. Carré, K. Termentzidis, and A. Tanguy, Ballistic heat transport in nanocomposite: The role of the shape and interconnection of nanoinclusions, Nanomaterials **11**, 1982 (2021).

[42] C. W. Chang, D. Okawa, H. Garcia, A. Majumdar, and A. Zettl, Breakdown of Fourier's Law in Nanotube Thermal Conductors, Phys. Rev. Lett. **101**, 075903 (2008).

[43] J. A. Johnson, A. A. Maznev, J. Cuffe, J. K. Eliason, A. J. Minnich, T. Kehoe, C. M. Torres, G. Chen, and K. A. Nelson, Direct Measurement of Room-Temperature Nondiffusive Thermal Transport over Micron Distances in a Silicon Membrane, Phys. Rev. Lett. **110**, 025901 (2013).

[44] X. Xu, L. F. Pereira, Y. Wang, J. Wu, K. Zhang, X. Zhao, S. Bae, C. T. Bui, R. Xie, J. T. Thong, B. H. Hong, K. P. Loh, D. Donadio, B. Li, and B. Ozyilmaz, Length-dependent thermal conductivity in suspended single-layer graphene, Nat. Commun. **5**, 3689 (2014).

[45] T. K. Hsiao, B. W. Huang, H. K. Chang, S. C. Liou, M. W. Chu, S. C. Lee, and C. W. Chang, Micron-scale ballistic thermal conduction and suppressed thermal conductivity in heterogeneously interfaced nanowires, Phys. Rev. B **91**, 035406 (2015).

[46] G. Hwang and O. Kwon, Measuring the size dependence of thermal conductivity of suspended graphene disks using null-point scanning thermal microscopy, Nanoscale **8**, 5280 (2016).

[47] A. El Sachat, F. Konemann, F. Menges, E. Del Corro, J. A. Garrido, C. Torres, F. Alzina, and B. Gotsmann, Crossover from ballistic to diffusive thermal transport in suspended graphene membranes, 2D Mater. **6**, 025034 (2019).

[48] R. Peierls, Zur kinetischen Theorie der Wärmeleitung in Kristallen, Ann. Phys. (Berlin, Ger.) **395**, 1055 (1929).

[49] V. Chiloyan, L. Zeng, S. Huberman, A. A. Maznev, K. A. Nelson, and G. Chen, Variational approach to solving the spectral Boltzmann transport equation in transient thermal grating for thin films, J. Appl. Phys. **120**, 025103 (2016).

[50] S. Huberman, R. A. Duncan, K. Chen, B. Song, V. Chiloyan, Z. Ding, A. A. Maznev, G. Chen, and K. A. Nelson, Observation of second sound in graphite at temperatures above 100 K, Science **364**, 375 (2019).

[51] Z. Zhang, Y. Ouyang, Y. Cheng, J. Chen, N. Li, and G. Zhang, Size-dependent phononic thermal transport in low-dimensional nanomaterials, Phys. Rep. **860**, 1 (2020).

[52] Z. Zhang, Y. Guo, M. Bescond, J. Chen, M. Nomura, and S. Volz, Heat Conduction Theory Including Phonon Coherence, Phys. Rev. Lett. **128**, 015901 (2022).

[53] W. M. Deen, *Analysis of Transport Phenomena* (Oxford University Press, New York, 1998).

[54] I. A. Kunin, *Elastic Media with Microstructure. I. One-Dimensional Models*, Springer Series in Solid-State Sciences Vol. 26 (Springer, Berlin, Heidelberg, 1982).

[55] J. N. Maki and T. Kodama, Phenomenological Quantization Scheme in a Nonlinear Schrödinger Equation, Phys. Rev. Lett. **57**, 2097 (1986).

[56] A. D. Martin, C. S. Adams, and S. A. Gardiner, Bright solitary-matter-wave collisions in a harmonic trap: Regimes of solitonlike behavior, Phys. Rev. A **77**, 013620 (2008).

[57] S. N. Gavrilov, A. M. Krivtsov, and D. V. Tsvetkov, Heat transfer in a one-dimensional harmonic crystal in a viscous environment subjected to an external heat supply, Continuum Mech. Thermodyn. **31**, 255 (2019).

[58] I. E. Berinskii and V. A. Kuzkin, Equilibration of energies in a two-dimensional harmonic graphene lattice, Philos. Trans. R. Soc. A **378**, 20190114 (2019).

[59] V. A. Kuzkin, Unsteady ballistic heat transport in harmonic crystals with polyatomic unit cell, Continuum Mech. Thermodyn. **31**, 1573 (2019).

[60] S. N. Gavrilov and A. M. Krivtsov, Steady-state kinetic temperature distribution in a two-dimensional square harmonic scalar

lattice lying in a viscous environment and subjected to a point heat source, Continuum Mech. Thermodyn. **32**, 41 (2020).

[61] V. A. Kuzkin and A. M. Krivtsov, Ballistic resonance and thermalization in the Fermi-Pasta-Ulam-Tsingou chain at finite temperature, Phys. Rev. E **101**, 042209 (2020).

[62] E. A. Korznikova, V. A. Kuzkin, A. M. Krivtsov, D. Xiong, V. Gani, A. A. Kudreyko, and S. V. Dmitriev, Equilibration of sinusoidal modulation of temperature in linear and nonlinear chain, Phys. Rev. E **102**, 062148 (2020).

[63] A. A. Sokolov, W. H. Müller, A. V. Porubov, and S. N. Gavrilov, Heat conduction in 1D harmonic crystal: Discrete and continuum approaches, Int. J. Heat Mass Transfer **176**, 121442 (2021).

[64] A. M. Krivtsov and A. S. Murachev, Transition to thermal equilibrium in a crystal subjected to instantaneous deformation, J. Phys.: Condens. Matter **33**, 215403 (2021).

[65] O. S. Loboda, E. A. Podolskaya, D. V. Tsvetkov, and A. M. Krivtsov, On the fundamental solution of the heat transfer problem in one-dimensional harmonic crystals, Continuum Mech. Thermodyn. **33**, 485 (2021).

[66] A. Y. Panchenko, V. A. Kuzkin, and I. E. Berinskii, Unsteady ballistic heat transport in two-dimensional harmonic graphene lattice, J. Phys.: Condens. Matter **34**, 165402 (2022).

[67] S. D. Liazhkov and V. A. Kuzkin, Unsteady two-temperature heat transport in mass-in-mass chains, Phys. Rev. E **105**, 054145 (2022).

[68] A. M. Krivtsov, Dynamics of matter and energy, Z. Angew. Math. Mech. **103**, e202100496 (2022).

[69] J. Lekner, *Theory of Reflection: Reflection and Transmission of Electromagnetic, Particle and Acoustic Waves* (Springer, Switzerland, 2016).

[70] J. Lekner, Energy, momentum, and angular momentum of sound pulses, J. Acoust. Soc. Am. **142**, 3428 (2017).

[71] A. B. Plachenov, P. Chamorro-Posada, and A. P. Kiselev, Nonparaxial tilted waveobjects, J. Lightwave Technol. **41**, 2212 (2023).

[72] C. Gomez-Reino, M. V. Perez, and C. Bao, *Gradient-Index Optics: Fundamentals and Applications* (Springer, Berlin, Heidelberg, 2002).

[73] D. R. Smith, J. J. Mock, A. F. Starr, and D. Schurig, Gradient index metamaterials, Phys. Rev. E **71**, 036609 (2005).

[74] V. M. Babich and V. S. Buldyrev, *Asymptotic Methods in Short-Wavelength Diffraction Theory* (Alpha Science International, Oxford, 2009).